Research article

Maize Sciences, 2026, 1: 100018

Phenotypic Characterization and Genetic Mapping of the Maize Lesion Mimic Mutant *Zmslmm* with Enhanced Disease Resistance to Multiple Pathogens

Meida DU[1,2], Chuang LIU[1,2], Jiaqi BAI[1,2], Shengfeng HE[1,3], Junbin CHEN[1,2], Xiaofan QI[4], Guozhi BI[4], Wangsheng ZHU[1,2]

([1]*State Key Laboratory of Maize Bio-breeding, China Agricultural University, Beijing 100193, China;* [2]*College of Plant Protection, China Agricultural University, Beijing 100193, China;* [3]*College of Agronomy and Biotechnology, China Agricultural University, Beijing 100193, China;* [4]*State Key Laboratory of Plant Environmental Resilience, College of Biological Sciences, China Agricultural University, Beijing 100193, China*)

Abstract: Lesion mimic mutants (LMMs) provide valuable resources for understanding plant immunity and disease resistance. Here, we characterized a spontaneous maize LMM, *Zmslmm*, in the KN5585 background, which exhibits elevated H_2O_2 accumulation, constitutive defense activation, and enhanced resistance to southern corn rust (SCR) and banded leaf and sheath blight (BLSB). Transcriptome profiling showed that defense-associated reprogramming preceded visible lesion formation and intensified after lesion development, accompanied by increased salicylic acid (SA) and lignin accumulation. Genetic analysis showed that the lesion-mimic phenotype is controlled by a single recessive locus in the KN5585 background. However, bulked segregant analysis (BSA) using an F_2 segregating population derived from *Zmslmm* and B73 identified three major loci, indicating genetic-background dependence of the *Zmslmm* phenotype in the B73 background. Together, these findings establish *Zmslmm* as a valuable genetic resource for understanding the coordination of immune activation, spontaneous cell death, and disease resistance in maize and provide a potential genetic resource for the improvement of disease resistance.

Key words: maize (*Zea mays* L.); lesion mimic mutants (LMMs); cell death; disease resistance; BSA mapping; transcriptional reprogramming

INTRODUCTION

Plants have evolved multilayered immune systems that recognize pathogen-derived or damage-associated signals and activate coordinated defense responses, including reactive oxygen species (ROS) production, transcriptional reprogramming, defense hormone signaling, and the accumulation of antimicrobial compounds. In many incompatible plant-pathogen interactions, these responses are accompanied by the hypersensitive response (HR), a localized form of programmed cell death that is often associated with the restriction of pathogen growth and spread (Lorrain et al., 2003; Jones and Dangl, 2006; Bruggeman et al., 2015). Lesion mimic mutants (LMMs) spontaneously develop chlorotic or necrotic lesions resembling HR-associated cell death in the absence of pathogen infection or obvious injury and therefore provide valuable genetic systems for dissecting the mechanisms that coordinate cell death and plant immunity (Johal et al., 1995; Lorrain et al., 2003).

Genetic studies in *Arabidopsis thaliana* and rice have revealed diverse molecular mechanisms underlying lesion-mimic and autoimmune phenotypes. In *Arabidopsis*, *lsd1*, *acd2*, and *acd11* cause deregulated cell death associated with perturbations in ROS homeostasis, chlorophyll catabolism, and sphingolipid metabolism, respectively. In addition, *acd6* and *cpr5* exhibit constitutive activation of salicylic acid (SA)-associated defense responses, spontaneous cell death, and enhanced disease resistance (Dietrich et al., 1997; Bowling et al., 1997; Rate et al., 1999; Mach et al., 2000; Brodersen et al., 2002). The *hlm1* mutant, caused by disruption of the cyclic nucleotide-gated

Received: 18 September 2026; **Accepted:** 5 November 2026
Corresponding author: Wangsheng Zhu (wangshengzhu@cau.edu.cn)
©The Author(s) 2026. Published by Higher Education Press
This is an open access article under the CC BY license (http://creativecommons.org/licenses/by/4.0)
https://doi.org/10.2738/MS.2026.0018

channel CNGC4, exhibits spontaneous lesion formation, constitutive defense activation, and altered HR-associated resistance, further linking ion homeostasis to the regulation of cell death and immunity (Balagué et al., 2003). Similar mechanistic diversity is evident in rice. The LMMs *spl11* and *oscul3a* connect ubiquitin-dependent protein turnover with cell death and immune regulation, and both exhibit enhanced resistance to fungal and bacterial pathogens (Zeng et al., 2004; Liu et al., 2017). Defects in vesicle trafficking and ubiquitination-associated processes in *spl28* and *spl35* likewise trigger spontaneous HR-like cell death, constitutive defense responses, and enhanced resistance to rice blast and bacterial blight, or to both fungal and bacterial pathogens (Qiao et al., 2010; Ma et al., 2019). More recently, the dominant rice LMM *Hlm1* was shown to display spontaneous HR-like cell death, excessive ROS accumulation, constitutive pathogenesis-related (PR) gene expression, and enhanced resistance, with elevated *OsNRAT1* expression contributing to the lesion phenotype (Zhang et al., 2025b). Moreover, disruption of phospholipid biosynthesis in *rbl1* produces a lesion-mimic phenotype and broad-spectrum multipathogen resistance (Sha et al., 2023). Collectively, LMMs arise from diverse cellular defects but commonly converge on deregulated cell death and enhanced defense.

Maize is one of the earliest and most extensively studied systems for lesion mimic genetics, with over 200 *Les/les* loci estimated and many mutants showing strong developmental, environmental, and genetic-background dependence (Neuffer and Calvert, 1975; Johal et al., 1995; Negeri et al., 2013). The autoactive nucleotide-binding leucine-rich repeat (NLR) mutant *Rp1-D21* provides a well-characterized example of genetic-background-dependent cell death, as the severity of its HR-like lesion phenotype varies markedly among maize genetic backgrounds (Chintamanani et al., 2010). Genetic analyses using diverse maize germplasm have subsequently identified multiple modifier loci affecting *Rp1-D21*-mediated HR (Chaikam et al., 2011; Olukolu et al., 2014). Further molecular studies revealed multiple regulators of *Rp1-D21* activity, including HCT and CCoAOMT proteins, ZmNANMT, metacaspases, and ZmVPS23-like, which modulate HR through protein interaction, metabolic regulation, or altered subcellular localization of Rp1-D21 (Wang et al., 2015; Wang and Balint-Kurti, 2016; Luan et al., 2021; Li et al., 2023; Sun et al., 2023). More recently, ZmFBK1 and ZmBPM1 were shown to negatively regulate *Rp1-D21*-mediated defense by promoting autophagy-associated turnover of Rp1-D21 (Tang et al., 2026a, b). Together, these studies demonstrate that lesion-mimic cell death triggered by an autoactive NLR can be strongly shaped by genetic background and multiple molecular regulators, highlighting the importance of modifier loci in determining the expression of maize lesion mimic phenotypes.

Other maize LMMs arise from defects in tetrapyrrole or chlorophyll metabolism, including *Les22*, *lls1*, and *nec-t*, which exhibit spontaneous or light-dependent cell death associated with metabolic perturbation and ROS accumulation (Gray et al., 1997; Hu et al., 1998; Zhao et al., 2022). The *lls1* allele *les30* further shows defense activation before visible lesion formation and stronger defense-associated metabolic reprogramming thereafter (Li et al., 2022). More recently, *Les8* was characterized as a light-dependent dominant LMM with reduced chlorophyll content, activated defense and secondary-metabolic pathways, increased lignin and jasmonic acid accumulation, and enhanced resistance to *Curvularia* leaf spot and southern corn leaf blight (Li et al., 2024).

Despite their distinct genetic origins, maize LMMs commonly converge on defense-associated transcriptional and metabolic reprogramming. *Les4*, *Les10*, *Les17*, and *lls1/les30* show activation of programmed cell death-, defense-, and phenylpropanoid-related pathways, often accompanied by altered photosynthesis and increased lignin accumulation (Mu et al., 2021; Li et al., 2022). Consistently, phenylpropanoid metabolism and specialized metabolites contribute to maize immunity via components such as HCT, CCoAOMT proteins, ZmCCoAOMT2, and zealexin pathways (Wang et al., 2015; Wang and Balint-Kurti, 2016; Yang et al., 2017; Ding et al., 2020). The connection between cell death regulation and broad disease resistance is further illustrated by several maize immune regulators. *ZmMM1* regulates immunity- and cell death-associated transcriptional networks and confers resistance to northern leaf blight, gray leaf spot, and southern corn rust (SCR) (Wang et al., 2021). Similarly, maize FERONIA-like receptors (ZmFLRs) can induce cell death and positively regulate resistance to northern corn leaf blight, northern corn

leaf spot, anthracnose stalk rot, and southern corn leaf blight (Yu et al., 2022). Collectively, these findings link cell death, immune activation, and metabolic reprogramming to enhanced disease resistance in maize.

In this study, we characterized the maize LMM *Zmslmm*, which exhibits constitutive immune activation, enhanced disease resistance, and strong genetic-background dependence. Defense-associated transcriptional reprogramming preceded visible lesion formation, and genetic mapping identified candidate regions for the underlying locus. These findings provide a basis for dissecting the genetic control of cell death and immunity in maize.

RESULTS

Identification and physiological characterization of the maize lesion mimic mutant *Zmslmm*

During field propagation and evaluation of maize germplasm, we identified a spontaneous LMM in the KN5585 background, designated *Zmslmm* (*Zea mays Spontaneous Lesion Mimic Mutant*). Under field conditions, neither KN5585 nor *Zmslmm* exhibited obvious lesion-mimic symptoms at the V2 stage. By the V5 stage, conspicuous chlorotic spots and patches were evident on *Zmslmm* leaves, whereas no comparable symptoms were observed in KN5585 (Fig. S1). At a later developmental stage, 80-day-old *Zmslmm* plants displayed pronounced necrotic lesions on their leaves, in contrast to KN5585 plants (Fig. 1-A and -B). These observations demonstrate that the lesion-mimic phenotype was already evident during early vegetative development under field conditions, although the precise stage of symptom onset was not determined.

As ROS accumulation is a hallmark of lesion formation and HR-like cell death, we examined H_2O_2 accumulation by DAB staining. *Zmslmm* leaves exhibited substantially stronger brown staining than KN5585 leaves, indicating increased H_2O_2 accumulation in mutant tissues (Fig. 1-C). In parallel, the defense-related genes *ZmPR1* and *ZmPR10* were significantly upregulated in *Zmslmm* under non-infected conditions (Fig. 1-D). Moreover, the contents of chlorophyll a and chlorophyll b were significantly reduced in *Zmslmm* compared with KN5585 (Fig. 1-E), indicating altered chlorophyll homeostasis in the mutant. Similar physiological alterations were observed in 15-day-old seedlings: compared with KN5585, *Zmslmm* seedlings exhibited lesion-mimic symptoms, increased H_2O_2 accumulation, elevated *ZmPR1* expression, and reduced chlorophyll contents (Fig. S2). Together, these results characterize *Zmslmm* as a spontaneous maize LMM in which visible leaf lesions are associated with increased H_2O_2 accumulation, constitutive activation of defense-related gene expression, and reduced chlorophyll contents.

Zmslmm exhibits enhanced resistance to southern corn rust and banded leaf and sheath blight

To determine whether the constitutive defense activation observed in *Zmslmm* is associated with altered disease resistance, we evaluated its responses to *Puccinia polysora* and *Rhizoctonia solani*, the causal agents of SCR and banded leaf and sheath blight (BLSB). For SCR, KN5585 and *Zmslmm* seedlings were inoculated with *P. polysora*. At 10 days post-inoculation (dpi), *Zmslmm* leaves developed markedly fewer uredinia than KN5585, with a significantly lower uredinial density (Fig. 2-A), indicating enhanced resistance to SCR.

We next evaluated resistance to BLSB under field conditions. KN5585 and *Zmslmm* plants were inoculated with *R. solani*, and disease severity was assessed at 14 dpi. Compared with KN5585, *Zmslmm* exhibited significantly lower disease scores and shorter lesion lengths (Fig. 2-B and S3), indicating enhanced resistance to BLSB. Together, these results show that *Zmslmm* exhibits enhanced resistance to two distinct fungal pathogens, consistent with its constitutively activated defense state.

Transcriptome profiling reveals defense activation in *Zmslmm*

To investigate the molecular changes associated with lesion development and enhanced disease resistance in *Zmslmm*, we performed RNA sequencing (RNA-seq) using leaves collected at the V1 and V3 developmental stages from KN5585 and *Zmslmm* plants grown in a growth chamber. At the V1 stage, neither genotype displayed visible lesion-mimic symptoms, whereas characteristic lesions were clearly evident in *Zmslmm* at the V3 stage (Fig. S4-A). These two developmental stages represent pre-lesion and lesion-bearing stages, respectively, allowing us to examine transcriptional changes before and after the appearance of visible lesions.

After sequencing, a total of 658 695 942 clean

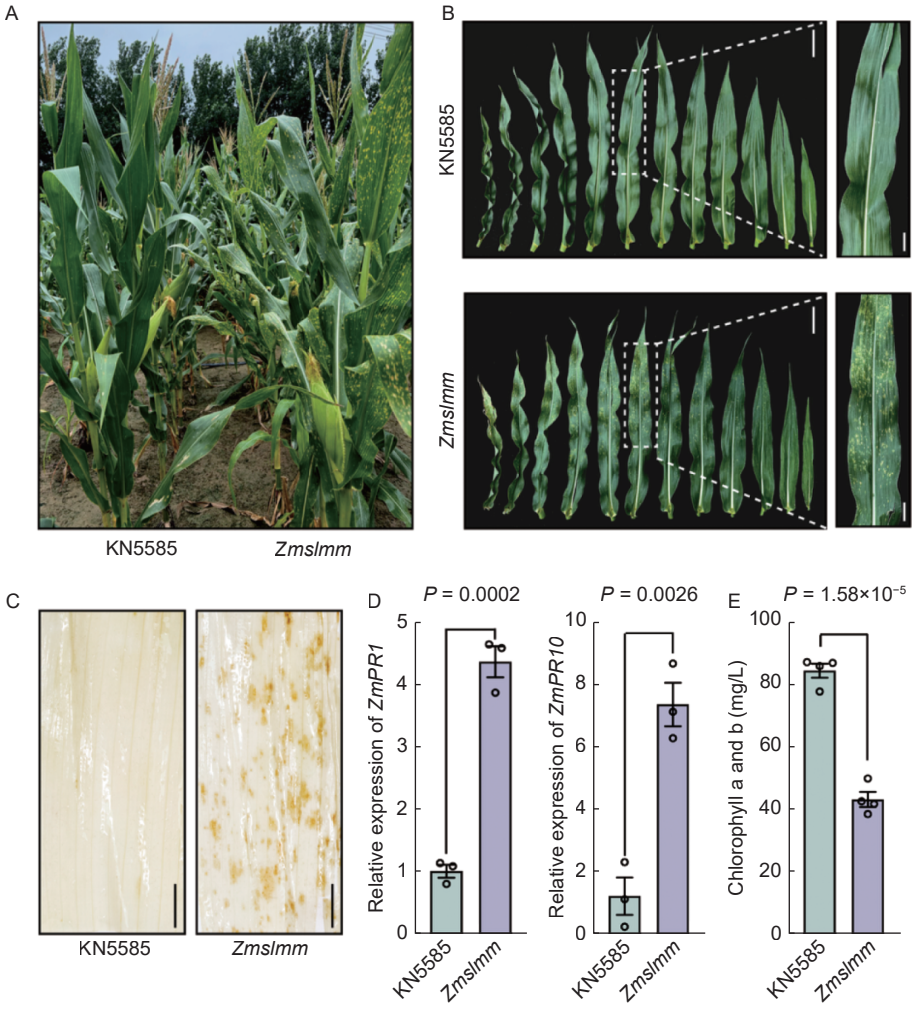


Fig. 1. Phenotypic and physiological characterization of field-grown *Zmslmm* plants.
A. Representative phenotypes of 80-day-old KN5585 and *Zmslmm* plants grown under field conditions. **B**. Representative leaves of KN5585 and *Zmslmm*, with enlarged views showing the lesion-mimic phenotype in *Zmslmm*. Scale bars, 10 cm for the whole-leaf images and 3 cm for the enlarged images. **C**. Representative DAB staining of H_2O_2 accumulation in KN5585 and *Zmslmm* leaves. Scale bars, 1 cm. **D**. Relative expression levels of *ZmPR1* (left) and *ZmPR10* (right) in non-inoculated KN5585 and *Zmslmm* leaves, as determined by reverse transcription-quantitative PCR (RT-qPCR). Bars represent mean ± SEM (n = 3). **E**. Chlorophyll a and chlorophyll b contents in KN5585 and *Zmslmm* leaves. Bars represent mean ± SEM (n = 4). Dots indicate individual biological replicates. Statistical significance was determined using two-tailed Student's t-tests, and exact P values are shown above the bars.

reads were obtained from the 16 resulting RNA-seq libraries (Table S2). Principal component analysis (PCA) clearly separated samples by genotype and developmental stage, with biological replicates clustering closely together (Fig. S4-B). Differential expression analysis identified 1312 differentially expressed genes (DEGs) between *Zmslmm* and KN5585 at the V1 stage, including 661 upregulated and 651 downregulated genes (Fig. 3-A and Dataset S1). At the V3 stage, 1775 DEGs were identified, comprising 931 upregulated and 844 downregulated genes (Fig. 3-A and Dataset S2). Gene Ontology (GO) enrichment analysis revealed that transcriptional changes associated with defense were already evident before visible lesion formation. At the V1 stage, DEGs were significantly enriched in GO categories related to response to SA, defense response to bacterium, response to biotic stimulus, and receptor kinase activity (Fig. 3-B and S4-C). At the V3 stage, immune-associated enrichment became more prominent, with significant enrichment of categories including defense response, response to SA, response to other organisms, and plant-type HR (Fig. 3-D). Consistent with these enrichment patterns, genes involved in defense response and SA response showed coordinated expression changes between *Zmslmm* and KN5585 (Fig. 3-C). Separate GO enrichment analyses of up- and downregulated DEGs

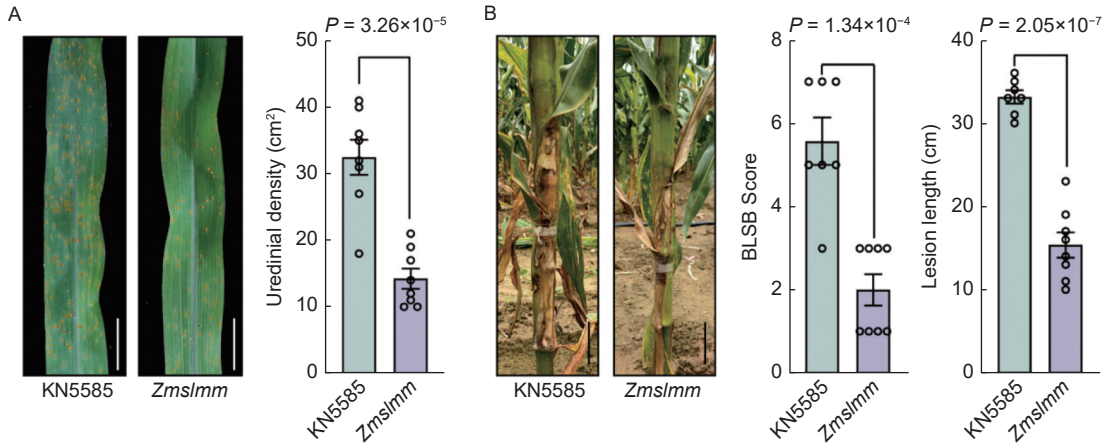


Fig. 2. *Zmslmm* exhibits enhanced resistance to southern corn rust and banded leaf and sheath blight.
A. Representative disease symptoms of KN5585 and *Zmslmm* seedling leaves inoculated with *Puccinia polysora* (left) and quantification of uredinial density (right) at 10 days post-inoculation. Scale bars, 1 cm. **B**. Representative BLSB symptoms of field-grown KN5585 and *Zmslmm* plants inoculated with *R. solani* (left), together with BLSB disease scores (middle) and lesion lengths (right) at 14 days post-inoculation. Scale bars, 5 cm. Bars represent mean ± SEM. Dots indicate individual biological replicates. Statistical significance was determined using two-tailed Student's *t*-tests, and exact *P* values are shown above the comparisons.

further showed that immune- and defense-related processes were predominantly enriched among genes upregulated in *Zmslmm* (Fig. S4-D). Collectively, these results demonstrate that defense-associated transcriptional reprogramming is already established in *Zmslmm* before the appearance of visible lesions and becomes more pronounced following lesion development, suggesting that immune activation precedes rather than simply results from macroscopic lesion formation.

To assess the reliability of the RNA-seq results, eight representative DEGs at the V3 stage were selected for RT-qPCR analysis. The expression patterns measured by RT-qPCR were broadly consistent with the RNA-seq results, supporting the reproducibility of the transcriptomic analysis (Fig. S5).

Elevated salicylic acid and lignin accumulation in *Zmslmm*

Given the enrichment of SA-associated processes revealed by transcriptome analysis, we examined the expression of SA biosynthesis-associated genes and quantified endogenous SA levels in KN5585 and *Zmslmm* leaves. The expression of *ZmSARD1*, a regulator of SA biosynthesis, and *ZmICS1*, a key gene involved in SA biosynthesis, was significantly upregulated in *Zmslmm* compared with KN5585 (Fig. 4-A). Consistent with these expression changes, *Zmslmm* leaves accumulated significantly higher levels of SA than KN5585 leaves (Fig. 4-B).

We further investigated lignin biosynthesis, which contributes to cell-wall reinforcement during plant defense. Transcriptome analysis revealed differential expression of multiple genes associated with this pathway (Fig. 4-D). Specifically, genes annotated as encoding cinnamoyl- CoA reductase (CCR; *Zm00001d011446*), a CCR-like protein (*Zm00001d046700*), a 4-coumarate CoA ligase-like protein (4CL-like; *Zm00001d030132*), and hydroxycinnamoyltransferase 11 (HCT11; *Zm00001d020530*) were significantly upregulated in *Zmslmm*. By contrast, another CCR gene, *Zm00001d044104*, was significantly downregulated, indicating that individual members of the same gene family differed in their transcriptional responses. Lignin quantification showed that lignin content was significantly higher in *Zmslmm* leaves than in KN5585 leaves (Fig. 4-C). Together, these results demonstrate increased SA and lignin accumulation in *Zmslmm*, accompanied by altered expression of genes associated with their biosynthesis.

Genetic analysis and bulked-segregant mapping of the *Zmslmm* phenotype

To investigate the genetic basis of the lesion-mimic phenotype, *Zmslmm* was crossed with its wild-type background KN5585 and with the maize inbred line B73. F_1 plants derived from the KN5585 × *Zmslmm* cross exhibited no visible lesion-mimic symptoms, resembling KN5585 rather than *Zmslmm* (Fig. S7). F_1 plants from both crosses were self-pollinated to generate F_2 populations. F_2 individuals were classified as normal-phenotype plants (NP) or mutant-

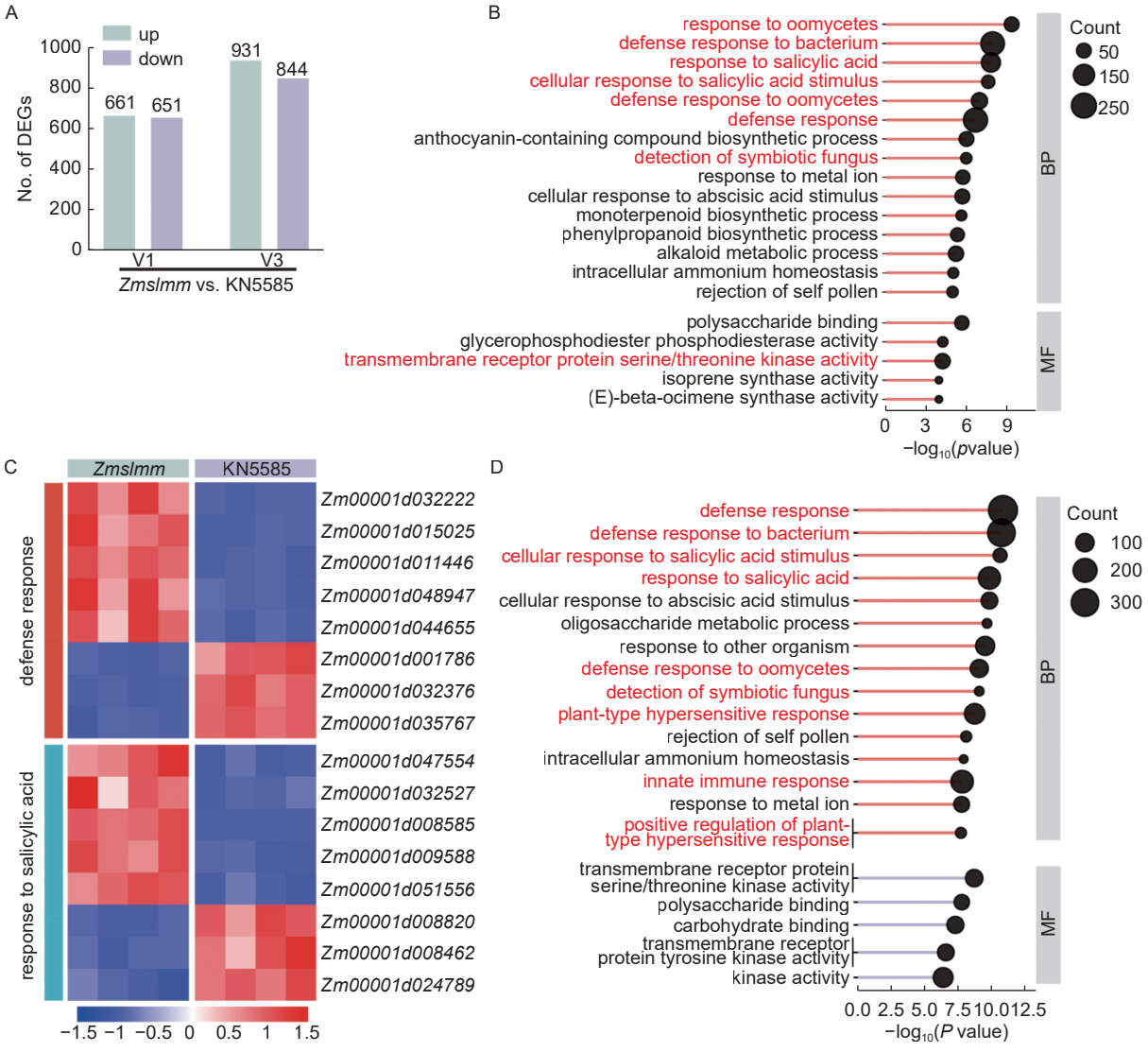


Fig. 3. Defense-associated transcriptional reprogramming in *Zmslmm*.

A. Numbers of up- and downregulated DEGs in *Zmslmm* relative to KN5585 at the V1 and V3 stages. DEGs were identified using DESeq2 with $|\log_2(\text{fold change})| > 1$ and an adjusted *P* value < 0.05. Four biological replicates were analyzed for each genotype at each developmental stage. **B**. GO enrichment analysis of DEGs between KN5585 and *Zmslmm* at the V1 stage. BP, biological process; MF, molecular function. Dot size represents the number of genes assigned to each GO term, and the x-axis indicates $-\log_{10}$ (*P* value). Defense- and immunity-related GO terms discussed in the main text are highlighted in red. **C**. Heatmap of genes associated with defense response and response to salicylic acid at the V3 stage. Red and blue indicate relatively high and low expression levels, respectively. Columns represent independent biological replicates. **D**. GO enrichment analysis of DEGs at the V3 stage. BP, biological process; MF, molecular function. Dot size represents the number of genes in each GO term, and the x-axis indicates $-\log_{10}$ (*P* value). Defense-related GO terms are highlighted in red.

phenotype plants (MP) based on the absence or presence of spontaneous lesion-mimic symptoms, respectively.

In the KN5585 × *Zmslmm* F_2 population, 147 plants exhibited the normal phenotype and 47 displayed the mutant phenotype, corresponding to an NP:MP ratio of 3.13:1.00. This segregation fitted the expected 3:1 ratio ($\chi^2 = 0.027$, $P > 0.05$; Table S3). Together with the absence of lesion-mimic symptoms in the F_1 plants, these results support inheritance of the phenotype through a single recessive locus in the KN5585 background. By contrast, the B73 × *Zmslmm* F_2 population comprised 533 normal and 36 mutant plants, with an NP:MP ratio of 14.81:1.00, which fitted a 15:1 segregation ratio ($\chi^2 = 0.0001$, $P > 0.05$; Table S3), suggesting that the expression of the mutant phenotype in the B73 background is controlled by two recessive genetic factors and likely requires homozygosity for recessive alleles at both loci. The contrasting segregation patterns between the two populations therefore indicate a pronounced effect of genetic background on the expression of the *Zmslmm*

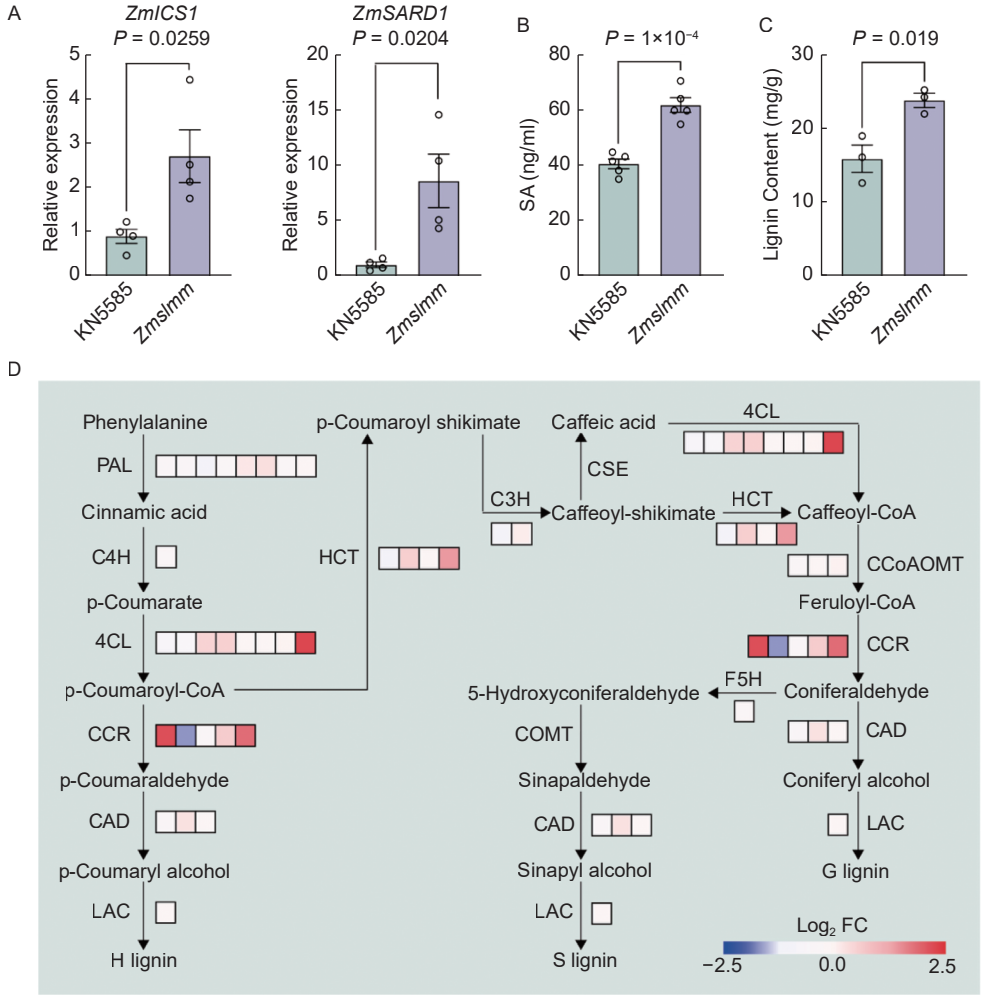


Fig. 4. Salicylic acid and lignin accumulation in *Zmslmm*.

A. Relative expression levels of *ZmICS1* (left) and *ZmSARD1* (right) in KN5585 and *Zmslmm* leaves determined by RT-qPCR. Expression levels were normalized to *Zm18S* and calculated using the $2^{-\Delta\Delta Ct}$ method. Bars represent mean ± SEM (n = 4), and dots indicate individual biological replicates. Statistical significance was determined using two-tailed Student's *t*-tests, and exact *P* values are shown above the bars. **B**. Salicylic acid (SA) content in KN5585 and *Zmslmm* leaves determined using a plant enzyme-linked immunosorbent assay (ELISA). The standard curve used for quantification is shown in Fig. S6-A. **C**. Lignin content in KN5585 and *Zmslmm* leaves quantified using an acetyl bromide (AcBr)-based lignin content assay kit. Bars represent mean ± SEM. Dots indicate individual biological replicates. Statistical significance was determined using two-tailed Student's *t*-tests, and exact *P* values are shown above the bars. **D**. Schematic of the lignin biosynthesis pathway showing transcriptomic changes in associated genes. Each square represents one gene annotated to the indicated enzyme family. Color denotes the Log_2 FC in *Zmslmm* relative to KN5585, ranging from -2.5 (blue) to +2.5 (red), with values near zero shown in white. When an enzyme family appears at multiple steps, the same set of genes is displayed at each corresponding step. The color coding represents transcript abundance and does not measure metabolic flux. PAL, phenylalanine ammonia-lyase; C4H, cinnamate 4-hydroxylase; 4CL, 4-coumarate CoA ligase; HCT, hydroxycinnamoyl; C3H, p-coumaroyl shikimate 3-hydroxylase; CSE, caffeoyl shikimate esterase; CCoAOMT, caffeoyl CoA O-methyltransferase; CCR, cinnamoyl CoA reductase; CAD, cinnamyl alcohol dehydrogenase; F5H, ferulate 5-hydroxylase; COMT, caffeic acid O-methyltransferase; LAC, laccase.

phenotype.

To map the loci associated with lesion formation, bulked segregant analysis (BSA) was performed using the B73 × *Zmslmm* F_2 population. Equal amounts of genomic DNA from mutant and normal F_2 individuals were combined to construct mutant and normal bulks, respectively, and the two bulks and their parental lines were subjected to whole-genome resequencing. In total, 2.12 billion clean reads comprising 315.77 Gb were obtained from the four libraries. Q30 values ranged from 97.60% to 97.90%; 91.70−97.80% of reads were properly paired, and 90−98% of the B73_v4 reference genome was covered, indicating that the sequencing data were suitable for subsequent association analysis. High-quality single-nucleotide polymorphisms (SNPs) and InDels that were polymorphic between the parents and reliably genotyped in the two bulks were retained for mapping.

Genome-wide ΔSNP-index, ΔInDel-index, and

G′ analyses identified multiple genomic regions associated with the lesion-mimic phenotype (Fig. 5). To improve mapping robustness, varFilter, varBScore, QTLseqr, and Euclidean distance (ED) analyses were independently applied to the sequencing data (Fig. 5 and S8; Tables S4, Table S5). The four methods identified partially overlapping but distinct sets of candidate regions. varFilter detected 16 intervals totaling 128.60 Mb on chromosomes 3, 4, 8, and 9; varBScore detected 61 intervals totaling 885.07 Mb across chromosomes 1−9; QTLseqr identified six intervals totaling 144.20 Mb on chromosomes 3, 4, 8, and 9; and ED analysis identified three intervals totaling 102.25 Mb on chromosomes 3 and 9. The variation in the number and extent of candidate intervals likely reflects differences in the statistical frameworks, thresholds, and sensitivities of these approaches.

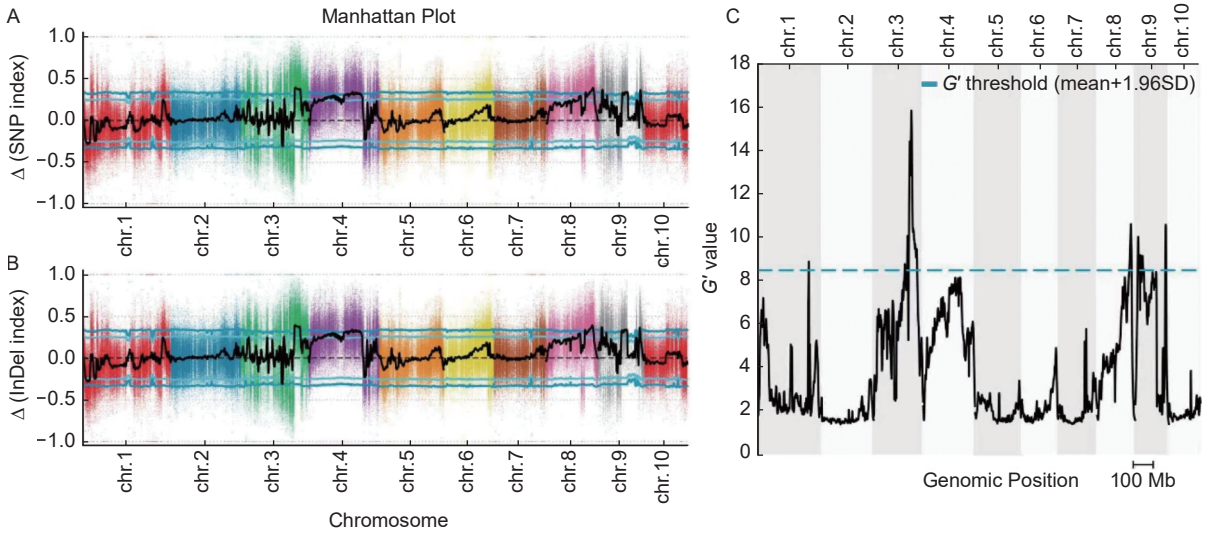


Fig. 5. Bulked-segregant analysis of the *Zmslmm* lesion-mimic phenotype in the B73 × *Zmslmm* F_2 population.
A. Genome-wide distribution of ΔSNP-index values between the normal and mutant F_2 bulks. SNP, single-nucleotide polymorphism. Colored dots represent individual SNPs, with colors distinguishing chromosomes. The black line represents the locally fitted ΔSNP-index trend, whereas the light blue and dark blue lines indicate the 95% and 99% confidence interval thresholds, respectively. **B**. Genome-wide distribution of ΔInDel-index values between the normal and mutant F_2 bulks. InDel, insertion/deletion. Colored dots represent individual InDels, the black line represents the locally fitted ΔInDel-index trend, and the light blue and dark blue lines indicate the 95% and 99% confidence interval thresholds. **C**. Genome-wide *G*′-value profile. The black line represents the smoothed *G*′ values across the genome, and the cyan dashed line indicates the significance threshold defined as the genome-wide mean *G*′ value plus 1.96 standard deviations. Alternating gray and white backgrounds indicate different chromosomes.

We therefore integrated the results from all four analyses and prioritized genomic regions supported by multiple independent methods. Three high-confidence candidate intervals were identified: 166.72−206.65 Mb on chromosome 3, 13.99−38.69 Mb on chromosome 9, and 84.14−96.22 Mb on chromosome 9 (Table S6). Comparison with previously reported maize lesion-mimic loci and mapped regions revealed that none of these three candidate intervals corresponded to previously reported loci or regions (Table S7). These three high-confidence candidate intervals represent the genomic regions most strongly associated with the *Zmslmm* lesion-mimic phenotype and provide priority targets for subsequent marker development, fine mapping, and identification of the underlying loci.

DISCUSSION

Zmslmm is a spontaneous maize LMM with progressive lesion formation, increased H_2O_2 accumulation, constitutive defense activation, reduced chlorophyll content, and enhanced resistance to SCR and BLSB (Figs. 1 and 2). Defense- and SA-associated transcriptional changes were detected before visible lesion formation at V1 and intensified at V3 (Figs. 3 and S4), indicating that immune activation precedes macroscopic cell death. This pattern is consistent with other LMMs, in which ROS accumulation, defense activation, spontaneous cell death, and disease resistance are closely associated (Lorrain et al., 2003; Bruggeman et al., 2015; Li et al., 2022; Mu et al., 2021; Fang et al., 2025).

The temporal transcriptomic patterns further support early immune activation in *Zmslmm*. At the V1 stage, defense- and SA-associated genes were already differentially expressed, and these responses became stronger at the V3 stage (Figs. 3 and S4),

resembling the pre-lesion defense activation reported for *les30* (Li et al., 2022). Consistently, *Zmslmm* accumulated more SA and showed increased expression of *ZmSARD1* and *ZmICS1* (Figs. 4-A and S6). The ICS1–SARD1/CBP60g module is central to SA biosynthesis and immune transcription (Wildermuth et al., 2001; Zhang et al., 2010; Wang et al., 2011; Sun et al., 2015; Ding et al., 2020; Peng et al., 2021), and SA metabolism also contributes directly to maize resistance to *R. solani* (Zhang et al., 2025a). In parallel, increased H_2O_2 accumulation and lignin content indicate that redox signaling and cell-wall reinforcement are activated simultaneously (Figs. 1-C and 4-B). ROS function as important signaling molecules in plant immunity but can also promote cell death when excessively accumulated (Apel and Hirt, 2004; Waszczak et al., 2018; Mittler et al., 2022), whereas lignification strengthens cell walls and restricts pathogen spread (Sattler and Funnell-Harris, 2013; Malinovsky et al., 2014; Barros et al., 2015; Lee et al., 2019). In maize, ZmFBL41-mediated regulation of ZmCAD links lignin accumulation directly to BLSB resistance (Li et al., 2019), while HCT and CCoAOMT proteins connect phenylpropanoid metabolism with immune regulation and quantitative disease resistance (Wang et al., 2015; Wang and Balint-Kurti, 2016; Yang et al., 2017). Collectively, SA signaling, ROS accumulation, and cell-wall reinforcement may constitute interconnected components of the constitutively activated defense state in *Zmslmm*, although their causal roles remain to be established.

The different segregation patterns in the two F_2 populations demonstrate a strong effect of genetic background on expression of the *Zmslmm* phenotype. In the KN5585 × *Zmslmm* F_2 population, the 3:1 segregation ratio indicates that the lesion-mimic phenotype is controlled by a single recessive locus in the KN5585 background. By contrast, the 15:1 ratio observed in the B73 × *Zmslmm* F_2 population is consistent with a two-locus recessive interaction in which lesion formation requires homozygosity for specific alleles at both loci (Table S3). A parsimonious model can represent the genotypes of *Zmslmm*, KN5585, and B73 as *aamm*, *AAmm*, and *AAMM*, respectively. Under this model, the second locus is fixed for the permissive *mm* genotype in *Zmslmm* and KN5585. Therefore, only the primary locus segregates in the KN5585-derived population, and *aamm* plants account for 1/4 of the F_2 progeny. In the B73-derived population, both loci segregate, and only *aamm* individuals are expected to develop lesions, resulting in a predicted mutant frequency of 1/16. The allele required at the second locus would thus have been introduced into the B73-derived population from the *Zmslmm* parent and may act as a recessive permissive modifier, whereas the corresponding B73 allele may suppress or complement expression of the lesion-mimic phenotype. This model provides a testable explanation for the observed segregation ratios but does not establish that the second-locus allele is a mutation specific to *Zmslmm*. Because *Zmslmm* originated in the KN5585 background, this allele could represent standing genetic variation shared with KN5585 rather than a second mutation that arose together with the primary lesion-mimic allele. Background-dependent modification of cell death has also been documented for *Rp1-D21*, for which multiple loci influence lesion severity (Chintamanani et al., 2010; Chaikam et al., 2011; Olukolu et al., 2014).

The three high-confidence intervals identified on chromosomes 3 and 9 do not overlap any previously reported maize lesion-mimic loci or mapped regions, indicating that *Zmslmm* may involve novel genetic determinants (Figs. 5 and S8; Tables S4 to S7). However, as both the primary causal locus and a putative background-dependent modifier may contribute to the phenotype in the B73-derived population, the genetic roles of these intervals remain to be resolved. Fine mapping in the KN5585- and B73-derived populations will enable the primary locus and modifier locus to be distinguished, while comparative whole-genome sequencing of KN5585, *Zmslmm*, and mutant F_2 individuals will facilitate the identification of candidate genes associated with lesion formation.

MATERIALS AND METHODS

Plant growth conditions

Seedling materials: All seeds were germinated on water-soaked blotting paper in shallow dishes at 25 °C in darkness for 3 days. Germinated seeds were selected for subsequent experiments.

Field-grown materials: All plants were grown under field conditions during the summer season at the Shangzhuang Experimental Station of China Agricultural University, Beijing, China.

Physiological and biochemical analyses

To detect H_2O_2 accumulation, three independent biological replicates from three different plants were used for each maize line. The freshly collected leaf samples were immersed in a 1 mg mL^{-1} 3,3′-diaminobenzidine (DAB) staining solution (pH 3.0) and incubated overnight in darkness. After staining, the leaves were transferred to a clearing solution containing ethanol, acetic acid, and glycerol at a volume ratio of 3:1:1 and boiled for 15 min; the solution was then replaced with fresh clearing solution, and the leaves were further decolorized at room temperature for at least 30 min. H_2O_2 in the leaf tissues reacted with DAB, resulting in the formation of brown precipitates. Stained leaves were photographed with a digital camera.

To determine chlorophyll content, leaf tissues from the same leaf position were collected from independent plants of each genotype. Three independent biological replicates were analyzed at the seedling stage (n = 3), and four independent biological replicates were analyzed at the adult stage (n = 4). Each biological replicate consisted of pooled leaf tissues from three independent plants, corresponding to a total of nine and twelve plants per genotype at the seedling and adult stages, respectively. Chlorophyll extraction and measurement were performed according to the method described by Qiu et al. (2016). Each biological replicate was measured in duplicate as technical replicates, and the mean of the technical measurements was used as the value of each biological replicate for statistical analysis.

Pathogen inoculation

For SCR inoculation, KN5585 and *Zmslmm* plants were grown to the V3 stage. Eight independent plants were used for each genotype. Fresh urediniospores were collected from infected maize leaves and suspended in sterile water containing 0.01% Tween-20 to a final concentration of approximately 1×10^6 spores mL^{-1}. The urediniospore suspension was evenly sprayed onto the leaf surfaces, whereas control plants were treated with 0.01% Tween-20 solution without urediniospores. After inoculation, plants were maintained under high humidity in darkness for 24 h to facilitate infection and subsequently transferred to normal growth conditions. Disease symptoms were evaluated at 10 dpi, with each individual plant considered an independent biological replicate.

For BLSB inoculation, twelve 6-mm-diameter mycelial plugs were collected from the edges of actively growing colonies and transferred to 200 mL of potato dextrose broth (PDB) in Erlenmeyer flasks. The cultures were incubated at 25 °C with shaking at 180 rpm for 3.5 days. Mycelia were then mechanically fragmented and used as inoculum. A 2-cm-wide strip of filter paper was saturated with the inoculum suspension, gently wrapped around the fourth leaf sheath of maize plants at the V9–V10 stage, and secured with grafting tape to maintain moisture. Seven KN5585 plants and eight *Zmslmm* plants were inoculated, with each individual plant considered an independent biological replicate. Lesion length and disease severity were evaluated at 14 dpi under field conditions.

Generation of mapping populations and bulkedsegregant analysis

To analyze the inheritance of the lesion-mimic phenotype, *Zmslmm* was crossed with KN5585 and B73, and F_2 populations were generated. F_2 individuals were classified as normal plants (NP) or mutant plants (MP) according to the presence or absence of spontaneous lesion-mimic symptoms, respectively. Segregation ratios were evaluated using chi-square tests against the expected Mendelian ratios.

For BSA, 36 mutant-phenotype and 40 normal-phenotype individuals were selected from the B73 × *Zmslmm* F_2 population. Genomic DNA was extracted separately from each individual, and equal amounts of DNA were pooled according to phenotype to generate the mutant and normal bulks, respectively. The two bulks, together with the parental lines B73 and *Zmslmm*, were subjected to whole-genome resequencing on the DNBSEQ-T7 platform. Raw reads were filtered using fastp (v0.23.4), and the resulting clean reads were aligned to the B73 RefGen_v4 reference genome using BWA-MEM. Genome-wide BSA signals were evaluated using four complementary approaches: varFilter, varBScore, QTLseqr, and ED analysis. Candidate genomic intervals supported by multiple approaches were integrated and prioritized for subsequent fine mapping.

RNA-seq and bioinformatic analyses

For transcriptome analysis, leaf tissues were collected from *Zmslmm* and KN5585 plants at the V1 and V3

stages. Neither genotype exhibited visible lesion-mimic symptoms at the V1 stage, whereas characteristic lesions were present in *Zmslmm* but absent from KN5585 at the V3 stage. Four independent biological replicates were analyzed for each genotype at each developmental stage. Samples were submitted to Tsingke Biotechnology (Beijing, China) for library construction and sequencing on the DNBSEQ platform. DEGs were identified using DESeq2 with $|\log_2(\text{fold change})| > 1$ and an adjusted $P < 0.05$. GO enrichment analysis was performed by Tsingke Biotechnology. GO terms with a false discovery rate (FDR) < 0.001 were considered significantly enriched, and the enrichment results were visualized using the online platform bioinformatics.com.cn.

RNA extraction and RT-qPCR

Total RNA was extracted from plant tissues using an RNA extraction kit (R401, Vazyme Biotech, Nanjing, China). First-strand cDNA was synthesized from 1 μg of high-quality total RNA (A260/A230 > 2.0 and A260/A280 > 1.8) using the HiScript III First Strand cDNA Synthesis Kit (R312, Vazyme Biotech, Nanjing, China) according to the manufacturer's instructions.

For RT-qPCR experiments, three or four independent biological replicates were analyzed for each genotype ($n \geq 3$), as specified in the corresponding figure legends, with each biological replicate consisting of leaf tissue collected from an independent plant. RT-qPCR was performed on an ABI QuantStudio 7 Flex Real-Time PCR System (Thermo Fisher Scientific) using SYBR Master Mix (Q711, Vazyme Biotech, Nanjing, China) according to the manufacturer's instructions. Each biological replicate was analyzed using two technical PCR replicates, and the mean Ct value of the two technical replicates was used for subsequent analysis. Relative transcript levels were calculated using the comparative Ct method ($2^{-\Delta\Delta Ct}$) (Livak et al., 2001), with *Zm18S* as the internal reference gene. The primers used for RT-qPCR are listed in Table S1.

RT-qPCR primer design and synthesis

Target-specific primers (18−25 nucleotides; annealing temperature, approximately 55 °C; amplicon size, 100−250 bp) were designed using NCBI Primer-BLAST based on maize coding sequences. Primers were designed to span exon-exon junctions or different exons, and their specificity was assessed against the maize reference genome. All primers were synthesized by Tsingke Biotechnology (Beijing, China).

Quantification of salicylic acid

To determine SA levels in KN5585 and *Zmslmm* plants, leaf tissues were collected from five 40-day-old plants per genotype, representing five biological replicates. Leaf tissues were extracted with 90% methanol at 4 °C overnight. The extracts were centrifuged at 4 °C, and the supernatants were collected and diluted 10-fold for subsequent analysis. SA content was determined using a plant SA ELISA kit (mlbio, Shanghai, China) according to the manufacturer's instructions. Each biological replicate was measured in two technical replicates, and the mean of the two technical measurements was used as the value of each biological replicate for subsequent statistical analysis. A standard curve was generated using GraphPad Prism 10, and the SA concentrations of the samples were calculated based on the standard curve.

Quantification of lignin

Total lignin content in maize leaves at the V3 stage was quantified using an acetyl bromide (AcBr)-based lignin content assay kit (Solarbio, BC4205) according to the manufacturer's instructions. Three independent biological replicates were analyzed for each genotype. Each biological replicate was measured in two technical replicates, and the mean of the two technical measurements was used as the value of each biological replicate for subsequent statistical analysis.

Statistical analysis

Unless otherwise indicated, data are presented as the mean ± standard error of the mean (SEM). Differences between two groups were evaluated using two-tailed Student's *t*-tests. Segregation ratios were evaluated using chi-square tests against the expected Mendelian ratios. Exact *P* values are reported in the figures, and $P < 0.05$ was considered statistically significant.

CONCLUSION

This study characterized *Zmslmm* as a spontaneous maize LMM with constitutive defense activation and enhanced resistance to SCR and BLSB. Defense-associated reprogramming preceded visible lesion

formation and was accompanied by increased SA and lignin accumulation, linking early immune activation to spontaneous cell death and disease resistance. Genetic analyses revealed strong background dependence and identified candidate genomic regions associated with lesion formation. These findings provide a basis for identifying the causal gene and modifier via fine mapping and functional validation.

ACKNOWLEDGEMENTS

This work was supported by the National Key Research and Development Program of China (No. 2025YFF1000302).

SUPPLEMENTAL DATA

Supplementary information is available at *Maize Sciences* online.

DECLARATION OF COMPETING INTEREST

The authors declare no conflict of interest.

REFERENCES

Apel K, Hirt H. 2004. REACTIVE OXYGEN SPECIES: Metabolism, oxidative stress, and signal transduction. *Annual Review of Plant Biology*, **55**: 373−399.

Balagué C, Lin B, Alcon C, et al. 2003. HLM1, an essential signaling component in the hypersensitive response, is a member of the cyclic nucleotide-gated channel ion channel family. *The Plant Cell*, **15**: 365−379.

Barros J, Serk H, Granlund I, et al. 2015. The cell biology of lignification in higher plants. *Annals of Botany*, **115**: 1053−1074.

Bowling S A, Clarke J D, Liu Y, et al. 1997. The *cpr5* mutant of Arabidopsis expresses both NPR1-dependent and NPR1-independent resistance. *The Plant Cell*, **9**(9): 1573−84.

Brodersen P, Petersen M, Pike H M, et al. 2002. Knockout of Arabidopsis accelerated-cell death11 encoding a sphingosine transfer protein causes activation of programmed cell death and defense. *Genes & Development*, **16**(4): 490−502.

Bruggeman Q, Raynaud C, Benhamed M, et al. 2015. To die or not to die? Lesions from lesion mimic mutants. *Frontiers in Plant Science*, **6**: 24.

Chaikam V, Negeri A, Dhawan R, et al. 2011. Use of mutant-assisted gene identification and characterization (MAGIC) to identify novel genetic loci that modify the maize hypersensitive response. *Theoretical and Applied Genetics*, **123**: 985−997.

Chintamanani S, Hulbert S H, Johal G S, et al. 2010. Identification of a maize locus that modulates the hypersensitive defense response, using mutant-assisted gene identification and characterization. *Genetics*, **184**: 813−825.

Dietrich R A, Richberg M H, Schmidt R, et al. 1997. A novel zinc finger protein is encoded by the Arabidopsis *LSD1* gene and functions as a negative regulator of plant cell death. *Cell*, **88**: 685−694.

Ding P, Ding Y. 2020. Stories of salicylic acid: A plant defense hormone. *Trends in Plant Science*, **25**: 549−565.

Fang C, Ma W, Zhu X, et al. 2025. Large-scale genomic deletion in *spl39* activates immune responses and confers resistance to rice bacterial blight. *Frontiers in Plant Science*, **16**: 1639365.

Gray J, Close P S, Briggs S P, et al. 1997. A novel suppressor of cell death in plants encoded by the *Lls1* gene of maize. *Cell*, **89**: 25−31.

Hu G, Yalpani N, Briggs S P, et al. 1998. A porphyrin pathway impairment is responsible for the phenotype of a dominant disease lesion mimic mutant of maize. *The Plant Cell*, **10**(7): 1095−1105.

Johal G S, Hulbert S H, Briggs S P. 1995. Disease lesion mimics of maize: A model for cell death in plants. *BioEssays*, **17**: 685−692.

Jones J D G, Dangl J L. 2006. The plant immune system. *Nature*, **444**: 323−329.

Lee M, Jeon H S, Kim S H, et al. 2019. Lignin - based barrier restricts pathogens to the infection site and confers resistance in plants. *The EMBO Journal*, **38**: EMBJ2019101948.

Li J, Chen M, Fan T, et al. 2022. Underlying mechanism of accelerated cell death and multiple disease resistance in a maize *lethal leaf spot 1* allele. *Journal of Experimental Botany*, **73**: 3991−4007.

Li J, Fan T, Zhang Y, et al. 2024. Characterization and fine mapping of a maize lesion mimic mutant (*Les8*) with enhanced resistance to *Curvularia* leaf spot and southern leaf blight. *Theoretical and Applied Genetics*, **137**: 7.

Li N, Lin B, Wang H, et al. 2019. Natural variation in ZmFBL41 confers banded leaf and sheath blight resistance in maize. *Nature Genetics*, **51**: 1540−1548.

Liu Q, Ning Y, Zhang Y, et al. 2017. *OsCUL3a* negatively regulates cell death and immunity by degrading OsNPR1 in rice. *The Plant Cell*, **29**: 345−359.

Lorrain S. 2003. Lesion mimic mutants: Keys for deciphering cell death and defense pathways in plants. *Trends in Plant Science*, **8**: 263−271.

Luan Q, Zhu Y, Ma S, et al. 2021. Maize metacaspases modulate the defense response mediated by the NLR protein Rp1 - D21 likely by affecting its subcellular localization. *The Plant Journal*, **105**: 151−166.

Livak K J, Schmittgen T D. 2001. Analysis of relative gene expression data using real-time quantitative PCR and the $2^{-\Delta\Delta CT}$ method. *Methods*, **25**(4): 402−408.

Li Y J, Gu J M, Ma S, et al. 2023. Genome editing of the susceptibility gene *ZmNANMT* confers multiple disease resistance without agronomic penalty in maize. *Plant Biotechnology Journal*, **21**(8): 1525−1527.

Ma J, Wang Y, Ma X, et al. 2019. Disruption of gene *SPL 35*, encoding a novel CUE domain - containing protein, leads to cell death and enhanced disease response in rice. *Plant Biotechnology Journal*, **17**: 1679−1693.

Mach J M, Castillo A R, Hoogstraten R, et al. 2000. The

Arabidopsis-accelerated cell death gene *ACD2* encodes red chlorophyll catabolite reductase and suppresses the spread of disease symptoms. *Proceedings of the National Academy of Sciences of the United States of America*, **98**(2): 771−6.

Malinovsky F G, Fangel J U, Willats W G T. 2014. The role of the cell wall in plant immunity. *Frontiers in Plant Science*, **5**: 178.

Mittler R, Zandalinas S I, Fichman Y, et al. 2022. Reactive oxygen species signalling in plant stress responses. *Nature Reviews Molecular Cell Biology*, **23**: 663−679.

Mu X, Li J, Dai Z, et al. 2021. Commonly and specifically activated defense responses in maize disease lesion mimic mutants revealed by integrated transcriptomics and metabolomics analysis. *Frontiers in Plant Science*, **12**: 638792.

Negeri A, Wang G F, Benavente L, et al. 2013. Characterization of temperature and light effects on the defense response phenotypes associated with the maize *Rp1-D21* autoactive resistance gene. *BMC Plant Biology*, **13**: 106.

Neuffer M G, Calvert O H. 1975. Dominant disease lesion mimics in maize. *Journal of Heredity*, **66**: 265−270.

Olukolu B A, Wang G F, Vontimitta V, et al. 2014. A genome-wide association study of the maize hypersensitive defense response identifies genes that cluster in related pathways. *PLoS Genetics*, **10**: e1004562.

Peng Y, Yang J, Li X, et al. 2021. Salicylic acid: Biosynthesis and signaling. *Annual Review of Plant Biology*, **72**: 761−791.

Qiu N, Wang X, Yang F, et al. 2016. Fast extraction and precise determination of chlorophyll. *Chinese Bulletin of Botany*, **51**(5): 667−678.

Qiao Y, Jiang W, Lee J, et al. 2010. *SPL28* encodes a clathrin - associated adaptor protein complex 1, medium subunit μ1 (AP1M1) and is responsible for spotted leaf and early senescence in rice (*Oryza sativa*). *New Phytologist*, **185**: 258−274.

Rate D N, Cuenca J V, Bowman G R, et al. 1999. The gain-of-function Arabidopsis *acd6* mutant reveals novel regulation and function of the salicylic acid signaling pathway in controlling cell death, defenses, and cell growth. *The Plant Cell*, **9**: 1695−708.

Sattler S E, Funnell-Harris D L. 2013. Modifying lignin to improve bioenergy feedstocks: Strengthening the barrier against pathogens. *Frontiers in Plant Science*, **4**: 70.

Sha G, Sun P, Kong X, et al. 2023. Genome editing of a rice CDP-DAG synthase confers multipathogen resistance. *Nature*, **618**: 1017−1023.

Sun T, Zhang Y, Li Y, et al. 2015. ChIP-seq reveals broad roles of SARD1 and CBP60g in regulating plant immunity. *Nature Communications*, **6**: 10159.

Sun Y, Ma S, Liu X, et al. 2023. The maize ZmVPS23-like protein relocates the nucleotide-binding leucine-rich repeat protein Rp1-D21 to endosomes and suppresses the defense response. *The Plant Cell*, **35**(6): 2369−2390.

Tang C X, Ma S J, Ge Q D, et al. 2026a. The F-box protein ZmFBK1 facilitates autophagy-mediated degradation of maize NLR protein Rp1-D21 to suppress the hypersensitive response. *Molecular Plant*, **19**(4): 784−803.

Tang C X, Liu T T, Ge Q D, et al. 2026b. The BTB/POZ-MATH protein ZmBPM1 interacts with autophagy-related protein ZmATG6 and modulates the NLR protein Rp1-D21-mediated defense response in maize. *Advanced Science*, e77193.

Wang G F, Balint-Kurti P J. 2016. Maize homologs of CCoAOMT and HCT, two key enzymes in lignin biosynthesis, form complexes with the NLR Rp1 protein to modulate the defense response. *Plant Physiology*, **171**: 2166−2177.

Wang G F, He Y, Strauch R, et al. 2015. Maize homologs of HCT, a key enzyme in lignin biosynthesis, bind the NLR Rp1 proteins to modulate the defense response. *Plant Physiology*, **169**: 2230−2243.

Wang H, Hou J, Ye P, et al. 2021. A teosinte-derived allele of a MYB transcription repressor confers multiple disease resistance in maize. *Molecular Plant*, **14**: 1846−1863.

Wang L, Tsuda K, Truman W, et al. 2011. *CBP60g* and *SARD1* play partially redundant critical roles in salicylic acid signaling. *The Plant Journal*, **67**: 1029−1041.

Waszczak C, Carmody M, Kangasjarvi J. 2018. Reactive oxygen species in plant signaling. *Annual Review of Plant Biology*, **69**: 209−236.

Wildermuth M C, Dewdney J, Wu G, et al. 2001. Isochorismate synthase is required to synthesize salicylic acid for plant defence. *Nature*, **414**: 562−565.

Yang Q, He Y, Kabahuma M, et al. 2017. A gene encoding maize caffeoyl-CoA O-methyltransferase confers quantitative resistance to multiple pathogens. *Nature Genetics*, **49**: 1364−1372.

Yu H, Ruan H, Xia X, et al. 2022. Maize FERONIA-like receptor genes are involved in the response of multiple disease resistance in maize. *Molecular Plant Pathology*, **23**: 1331−1345.

Zeng L R, Qu S, Bordeos A, et al. 2004. *Spotted leaf11*, a negative regulator of plant cell death and defense, encodes a U-Box/Armadillo repeat protein endowed with E3 ubiquitin ligase activity. *The Plant Cell*, **16**: 2795−2808.

Zhang Y, Xu S, Ding P, et al. 2010. Control of salicylic acid synthesis and systemic acquired resistance by two members of a plant-specific family of transcription factors. *Proceedings of the National Academy of Sciences*, **107**: 18220−18225.

Zhang C, Zhang H, Lin W, et al. 2025a. ZmDREB1A controls plant immunity via regulating salicylic acid metabolism in maize. *The Plant Journal*, **121**: e17226.

Zhang P, Zong C, Gu Y, et al. 2025b. Lesion mimic gene *HLM1* positively regulates cell death and disease resistance in rice. *Frontiers in Plant Science*, **16**: 1669235.

Zhao Y, Xu W, Wang L, et al. 2022. A maize necrotic leaf mutant caused by defect of coproporphyrinogen III oxidase in the porphyrin pathway. *Genes*, **13**: 272.